1.3: Test Measurements on a Steam Channel for Probe Calibration

by: D. Granser, Kraftwerk-Union AG., Mülheim-Ruhr

INTRODUCTION

Probes for measurements in steam turbines are usually calibrated in air. To correct for different isentropic coefficients in air and steam similarity rules are used (e.g. the von Karman rule). The problem is even more complicated in wet steam. It was therefore considered very useful to be able to calibrate in steam.

Notation

p'''	(mbar)	Total pressure
p''	(mbar)	Static pressure
ρ	(kg/m^3)	Density
U	(m/s)	Velocity
q	(mbar)	Dynamic head
η	(kg/m s)	Dynamic viscosity
κ =	1,325	Isentropic coefficient
B, H	(mm)	Breadth, height
M*		Laval number
M		Mach number
Re		Reynolds number

Indices

m	Average value
s	Probe
D	Nozzle
E	Inlet
^	Normal shock

DESCRIPTION OF THE STEAM CHANNEL

Up to 15 t/h saturated steam of about 10 bar are delivered by the central heat supply.

The steam facility at Kraftwerk Union consists of water-separator, superheater, control valve and steam cooler to provide steam of desired conditions for the interchangeable test rigs. The exhaust flow is ducted to a condenser and the condensate pumped back to the boiler feed tank.

One of these interchangeable test rigs is the steam channel for probe calibration which is shown in Fig. 1.3.1. Passing a honeycomb and up to three grids, the flow is homogenized. Boundary layer and waterfilm are removed through slots in the sidewalls of the rectangular section (150 × 260 mm^2). A series of fixed symmetrical nozzles are mounted in turn on the upper and lower wall. A small gap between nozzle inlet and wall is used to suck off the boundary layer and waterfilm. Nozzle design was based on superheated steam conditions. Each nozzle should give a parallel flow in the test section. The flow is guided by rigid sidewalls and behaves like a free jet on the upper and lower side. The test section has a cross sectional area of 150 × 150 mm^2. Windows made of quartz glass (160 Ø mm) for use in optical methods (Schlieren, interferometer) are mounted on the rigid sidewalls. Differently inclined holes (13 Ø mm) in the probe support system are equipped with ball valves and allow pitch angle changes during operation. The probe position and the yaw angle are changed by aid of a drive unit which is mounted on the probe support.

The exit of the test section is connected to a diffuser. To control the backpressure a butterfly valve and a control valve are located in the piping near the condenser.

First experiments showed the necessity of altering the design of the test section. The backpressure (pressure between free jet boundary and wall) is a function of area ratio between nozzle exit and channel; it is also influenced by the probeshaft. To avoid over expansion, plates were inserted to reduce the effective channel height and, to maintain the same backpressure, the upper and lower region of the channel were connected by pipes. An adjustable nozzle at the exit of the test section provides a better control of the backpressure. All the ducting is made of stainless steel to avoid corrosion.

INSTRUMENTATION

The total pressure was measured by a total-pressure probe mounted in the ducting ∿0.5 m upstream of the nozzle throat.

The static pressure was obtained from four tappings in the nozzle exit. The Laval number distribution in Laval nozzles can be calculated from static pressure and total pressure upstream or the pitot-pressure (pressure behind a normal shock) and the total pressure upstream.

In the present experiments the second method was chosen because it is more insensitive to variation in the incidence angle. Two pitot-probes used in the experiments are shown in Fig. 1.3.2. The static pressure distribution in the subsonic nozzle was obtained by a series of static pressure probes represented in Fig. 1.3.3. The arrangement of the pressure transducers is shown in Fig. 1.3.4. All connecting lines were purged by compressed air which was ducted through a steam-heated heat exchanger.

The set up of the Schlieren optics is represented in Fig. 1.3.5. The Schlieren system was mainly used to check the probes.

EXPERIMENTS

All nozzles were designed to give a parallel flow at the exit. To check the flow distribution in the test section, the subsonic nozzle and the Laval nozzles for M* = 1.3, 1.5, 1.7 were tested in superheated steam. The temperature chosen was as high as necessary to avoid expansion into the wet steam region. The boundary layer suction was adjusted to give a symmetrical total pressure profile at the nozzle inlet.

The fixed nozzles were mounted in turn in the steam channel. The measurements were performed in a meridional plane (Y/H = 0), the various probes moved in the vertical direction (X/H = const.).

At any desired point the readings were repeated three times with air-purging between; the results are averaged values.

Subsonic Nozzle:

To examine the total pressure distribution, the test section was traversed with a pitot-probe. The deviation from constant total pressure obtained was within the accuracy range of the pressure transducers.

The static pressure distribution was measured at three distances from the nozzle exit. The results are represented in Fig. 1.3.6 to 1.3.9. As one would expect the difference between static pressure measured with the probe and static pressure measured at the nozzle exit increases with distance. Table 1 shows the averaged pressure difference and the maximum deviation from constant static pressure distribution. To sort out the influence of M* - Re-number the total and static pressure were changed independently with the probe fixed at one position. For the results see Fig. 1.3.8. The values scatter around constant static pressure difference with a maximum deviation of $\pm 6.62 . 10^{-3}$. That means the static pressure distribution is independent of M* and Re-number in the range of $0.4 \leqslant M^* \leqslant 0.8$ and $5.10^5 \leqslant Re \leqslant 1.3.10^6$.

Laval Nozzles M* = 1.3, 1.5, 1.7

To calculate the M*-number distribution, the pitot-pressures were measured in the most relevant region of the test diamond. The results for the different nozzles are shown in Fig. 1.3.10 to 1.3.12. The averaged Laval numbers and the maximum deviations are represented in Table 2. The Laval numbers calculated from static pressures at the nozzle exit agree well with the averaged values obtained by pitot measurements. Repeated measurements showed maximum errors of ±1.12% for M* = 1.3 and ±0.75% for M* = 1.5. Hence the whole amount of Laval number deviations cannot be attributed to flow inhomogeneities. It is assumed that one major source is air-purging because it is very difficult to decide precisely when pressure equilibrium has occurred.

Mach number deviations for bigger wind tunnels in Göttingen (1000 × 1000 mm) and Braunschweig (500 × 500 mm) are given in references [2] and [3]. The maximum deviation is ±0.55% and ±1% respectively. Disturbances are a function of machining accuracy to channel height. An explanation for larger deviations could also be the comparatively small size of the channel presented in this paper.

REFERENCES

[1] WGL-Bericht Nr. 5/1962

[2] W- Lorenz-Meyer: Die Strahleigenschaften der Messstrecke des Transonischen Windkanals der AVA. Forschungsbericht 66 - 19

[3] H. Köster: Eichung des grossen Überschall-Windkanals der DFL (Messquerschnitt 50 × 50 cm^2). Forschungsbericht 67 - 95

APPENDIX

Definition of pressure coefficients:

$$^{\Delta}p''' = p''' - p_s'''$$

$$^{\Delta}p'' = p_D'' - p_s''$$

$$q = p''' - p_D''$$

$p'''/\hat{p}_s'''$ ratio as a function of M*:

$$\frac{p'''}{\hat{p}_s'''} = M^{*-2} \left[\frac{1 - \frac{\kappa-1}{\kappa+1} M^{*2}}{1 - \frac{\kappa-1}{\kappa+1} \frac{1}{M^{*2}}} \right]^{\frac{1}{\kappa-1}}$$

Re number definition:

$$Re = \frac{U \rho H}{\eta}$$

Tables 1-2, Fig. 1.3.1.-1.3.12 attached.

Table 1:

X/H	M^* (p''')	$\Delta p''_m/q$	$\sigma \Delta p''/q$
0,3267	0,4130	-0,03684	$\pm 6,6 \cdot 10^{-3}$
	0,6065	-0,03943	$\pm 8,19 \cdot 10^{-3}$
0,2533	0,66, 824mbar	-0,02501	$\pm 6,5 \cdot 10^{-3}$
	0,66, 685mbar	-0,02602	$\pm 6,42 \cdot 10^{-3}$
0,1533	0,4102	-0,00231	$\pm 4,47 \cdot 10^{-3}$
	0,6207	0,00023	$\pm 4,04 \; 10^{-3}$

Table 2:

Nozzle	M^*_m	$\frac{\Delta M^*}{M^*_m}$ [%]
1,3	1,3003	±1,51
1,5	1,5018	±1,21
1,7	1,6896	± 0,36

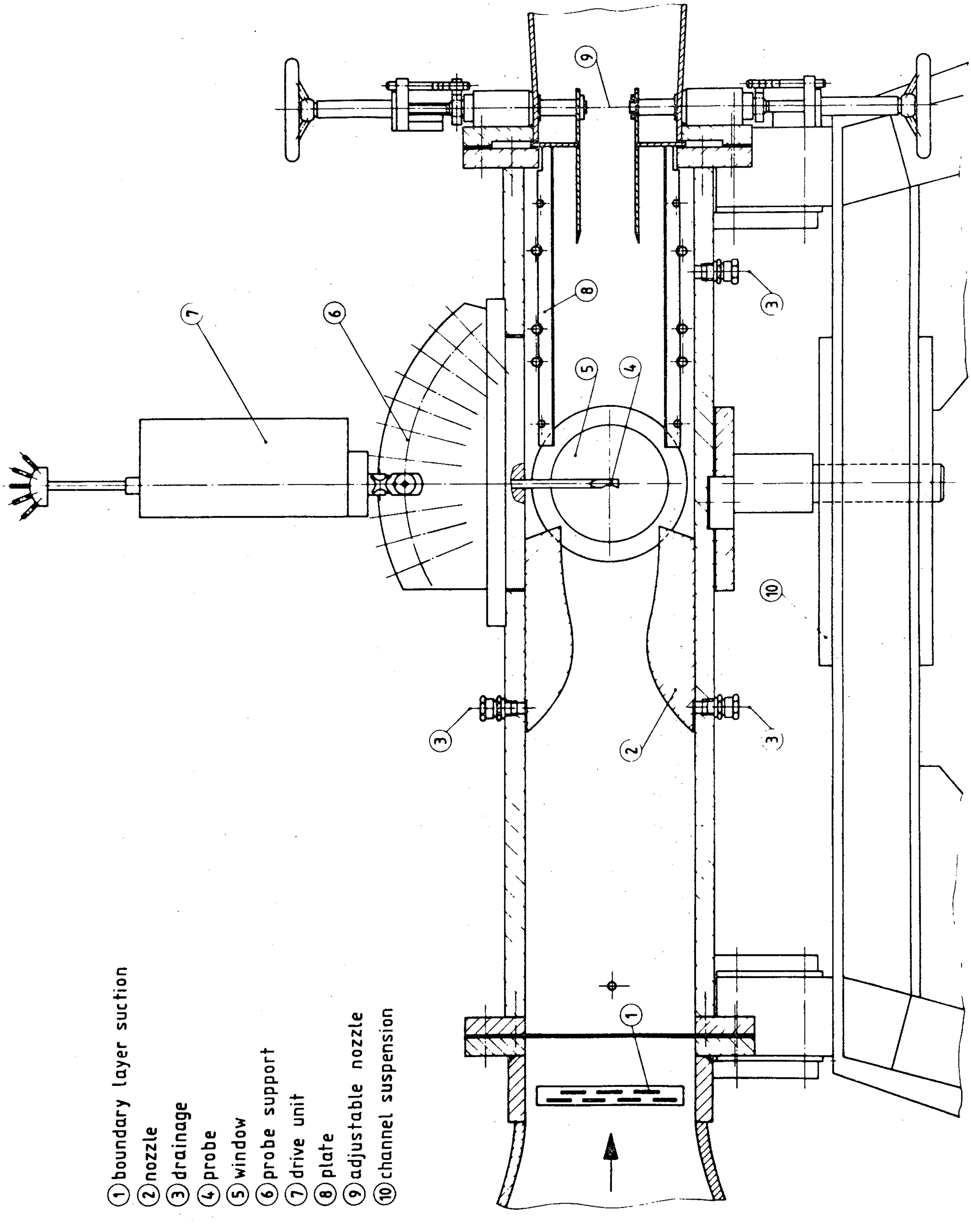

FIG. 1.3.1. STEAM CHANNEL

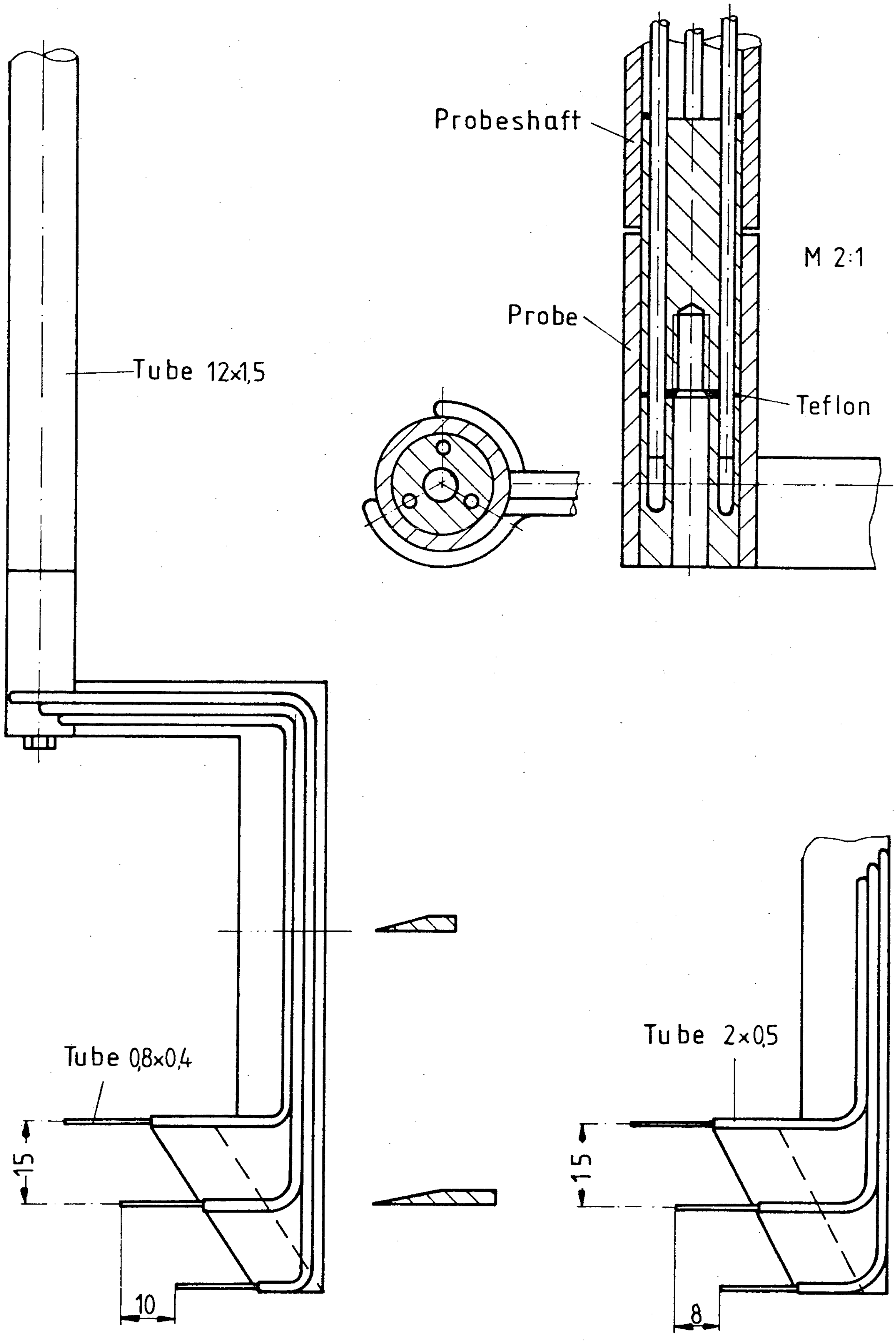

FIG. 1.3.2. PITOTPROBE AND CONNECTION

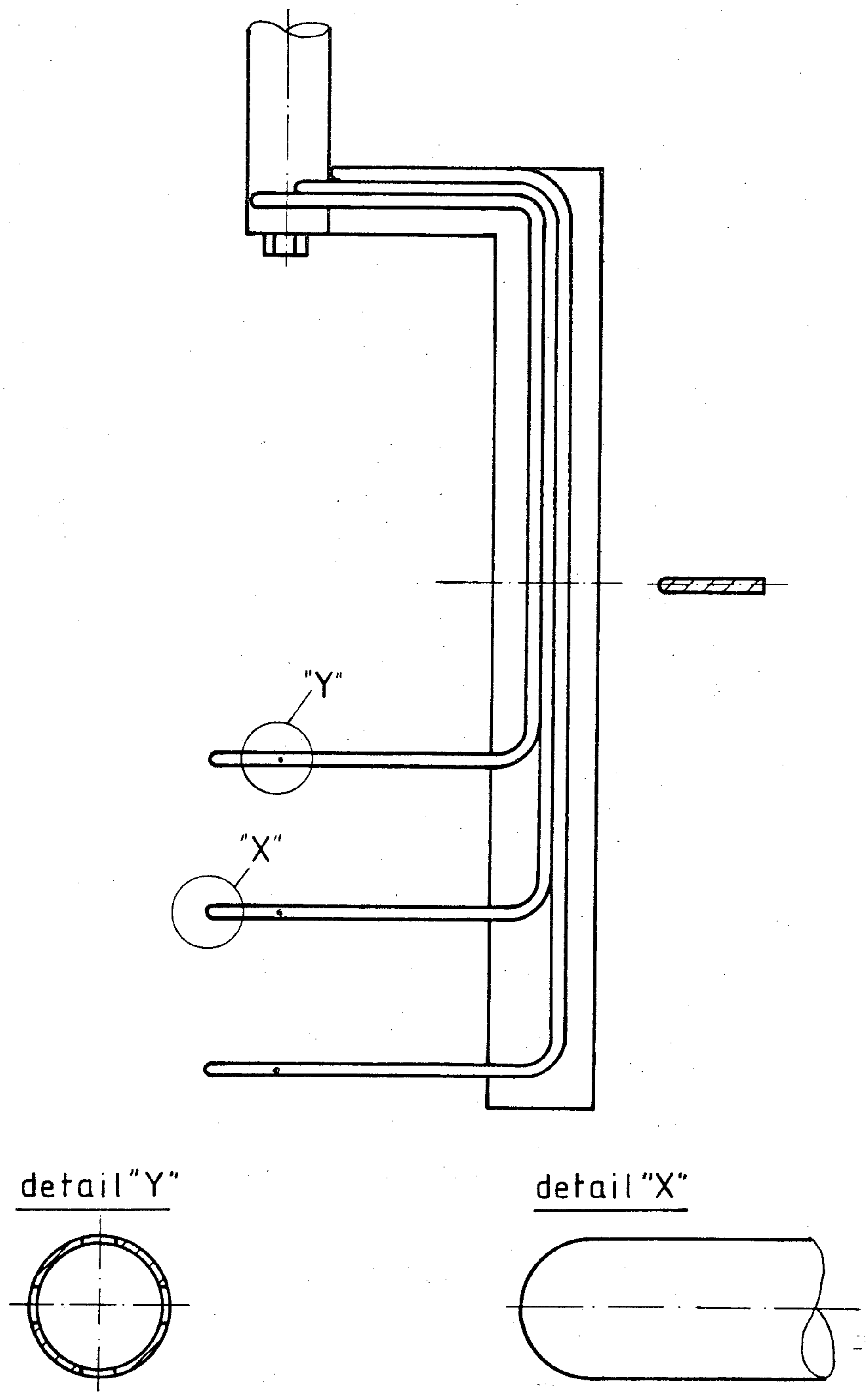

FIG. 1.3.3. STAT. PRESSURE PROBE

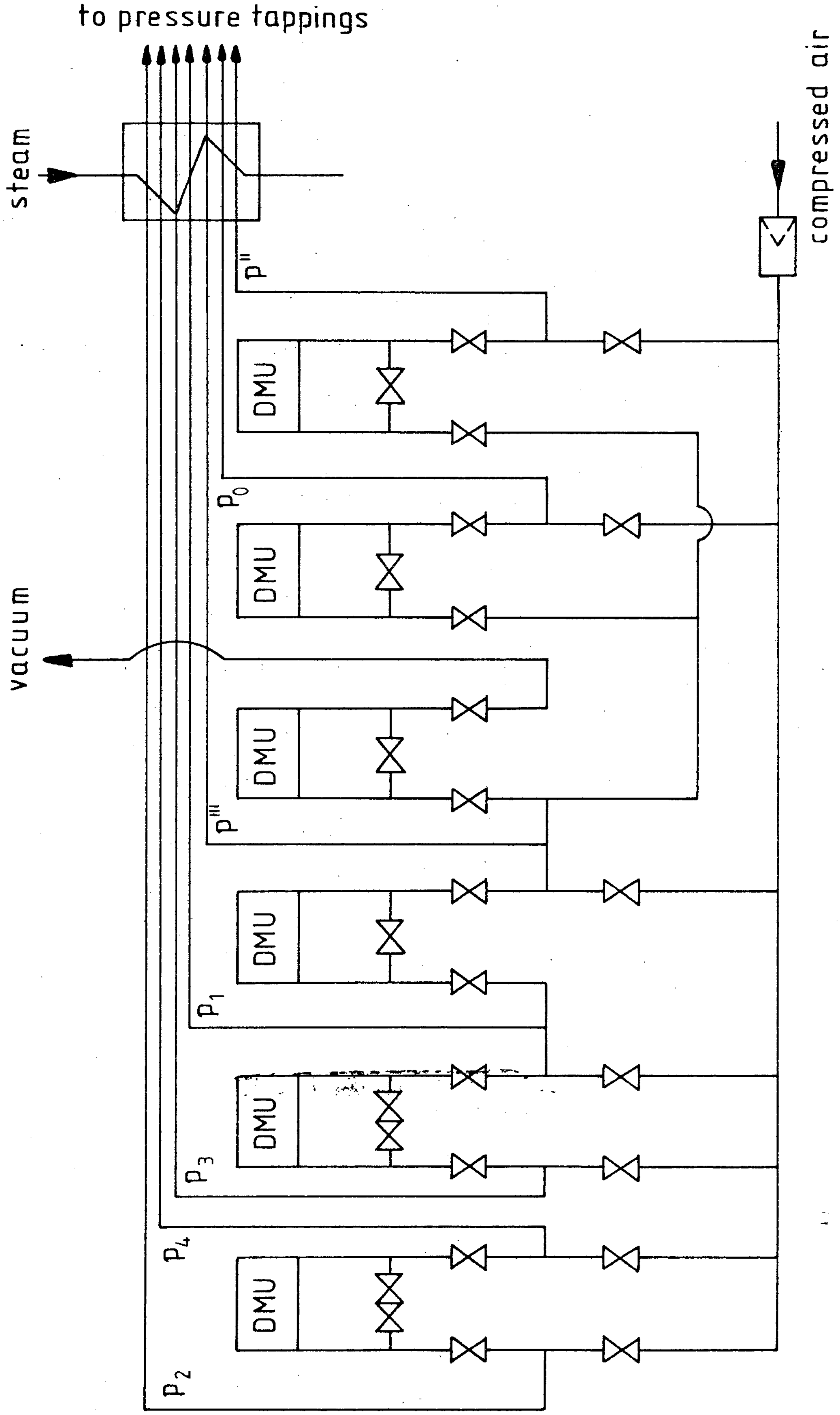

FIG. 1.3.4. INSTRUMENTATION

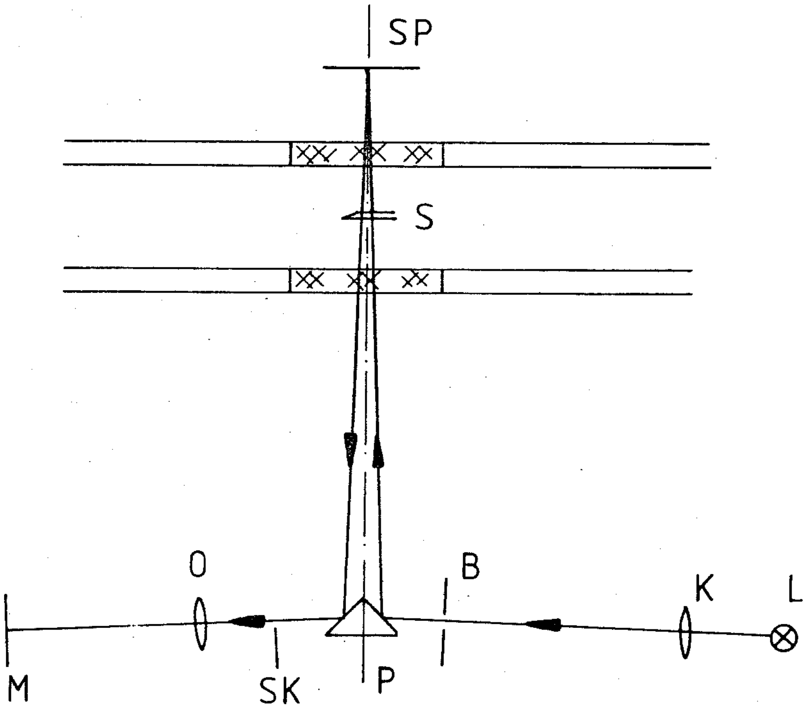

L lightsource
K condensorlens
B aperture
P prism

SP mirror
SK edge
O lens
M screen
S probe

FIG. 1.3.5. SCHLIERENOPTIC

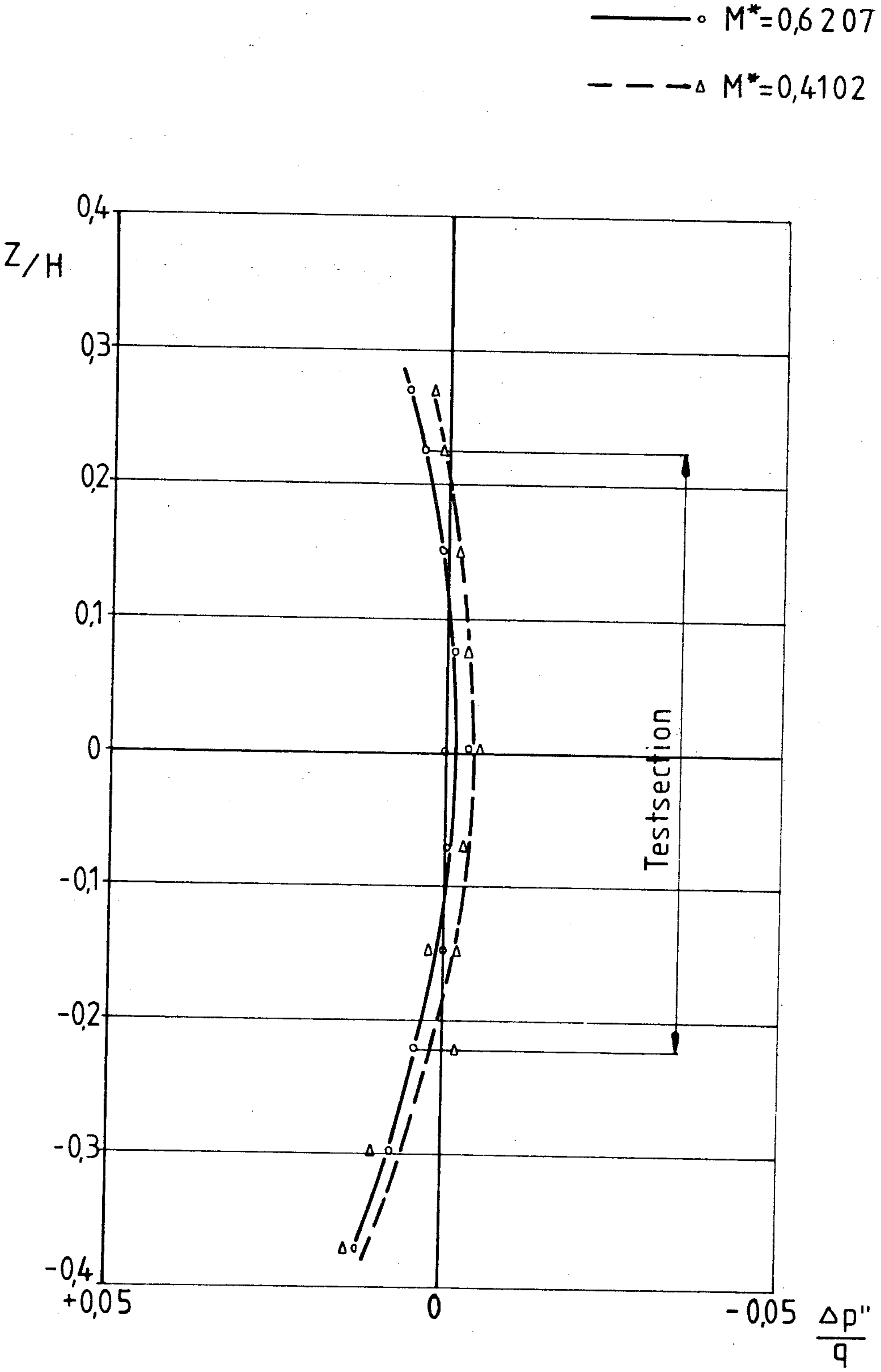

FIG. 1.3.6. SUBSONIC NOZZLE STAT. PRESSURE DISTRIBUTION X/H = 0,1533

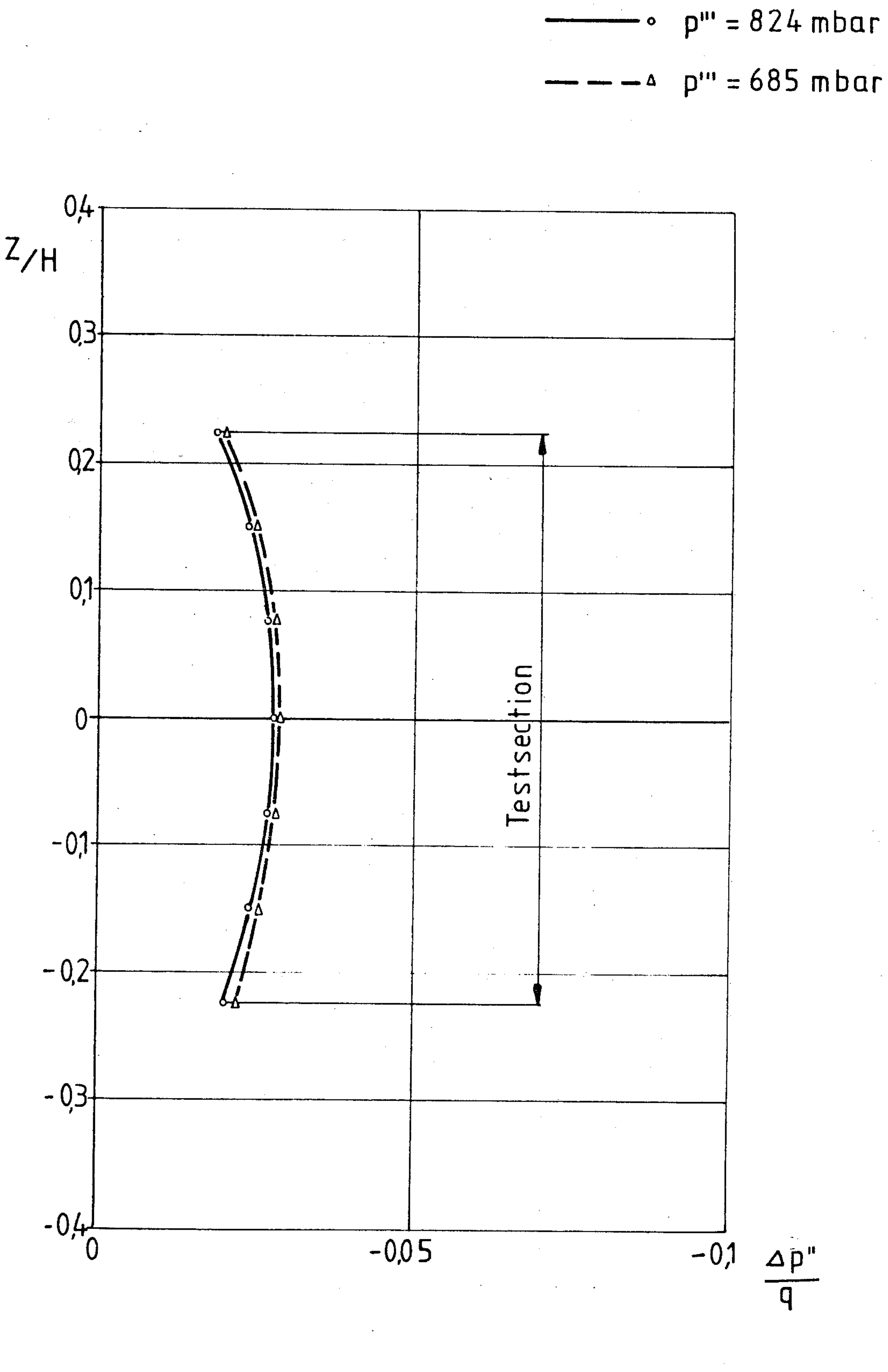

FIG. 1.3.7. SUBSONIC NOZZLE STAT. PRESSURE DISTRIBUTION X/H = 0,2533 M* = 0,66

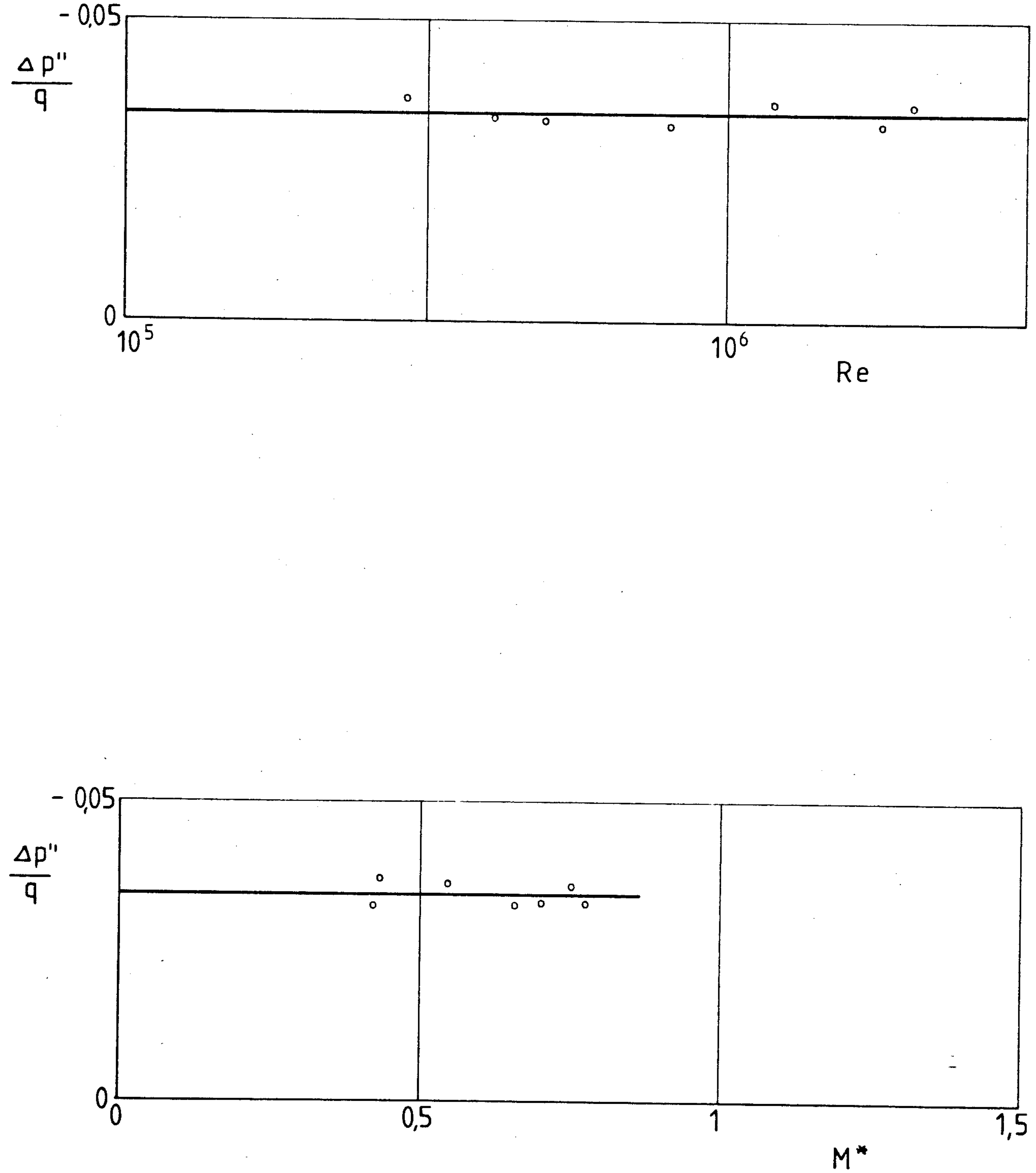

FIG. 1.3.8. SUBSONIC NOZZLE STAT. PRESSURE VERSUS Re AND M*

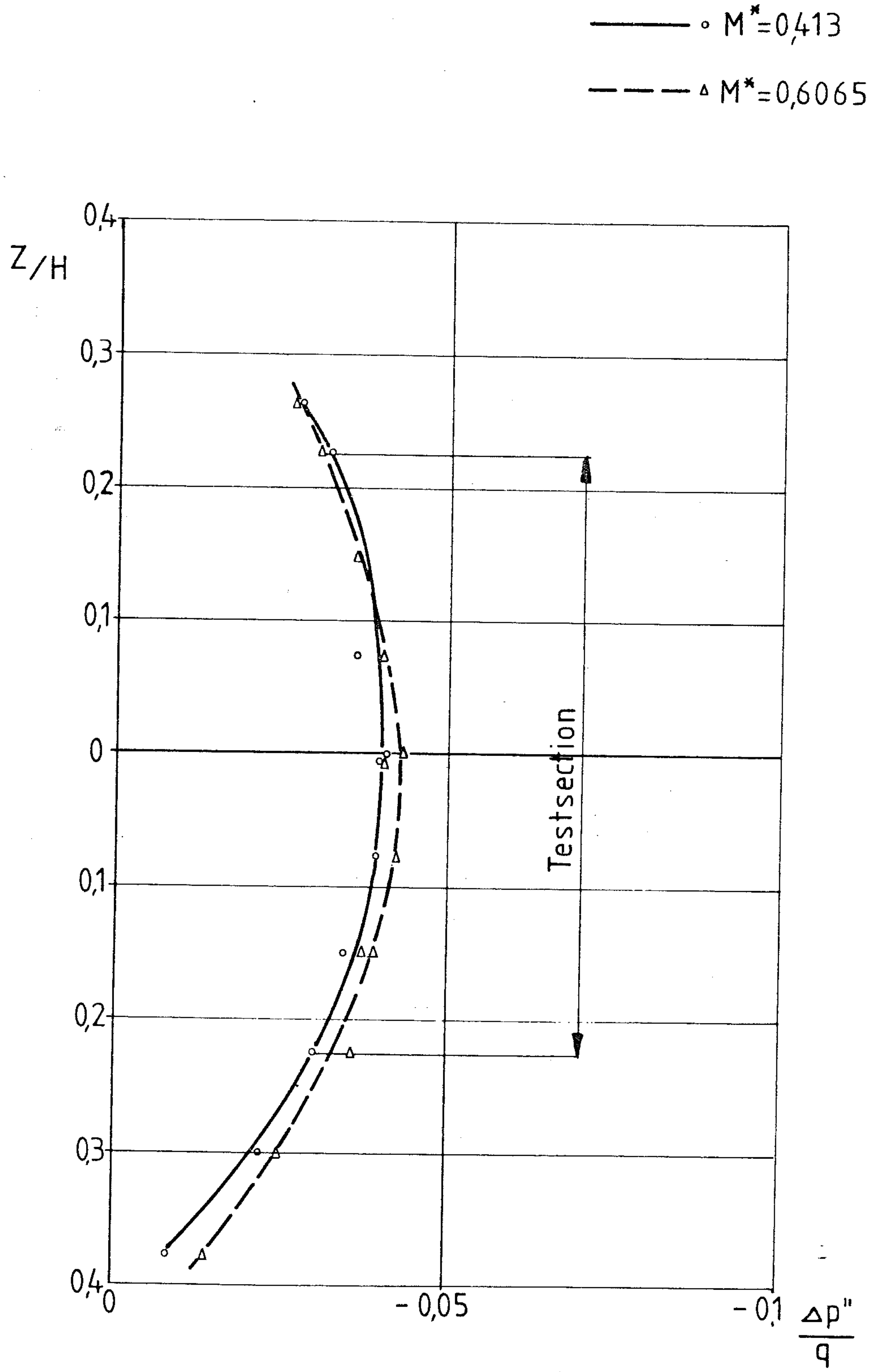

FIG. 1.3.9. SUBSONIC NOZZLE STAT. PRESSURE DISTRIBUTION X/H = 0,3267

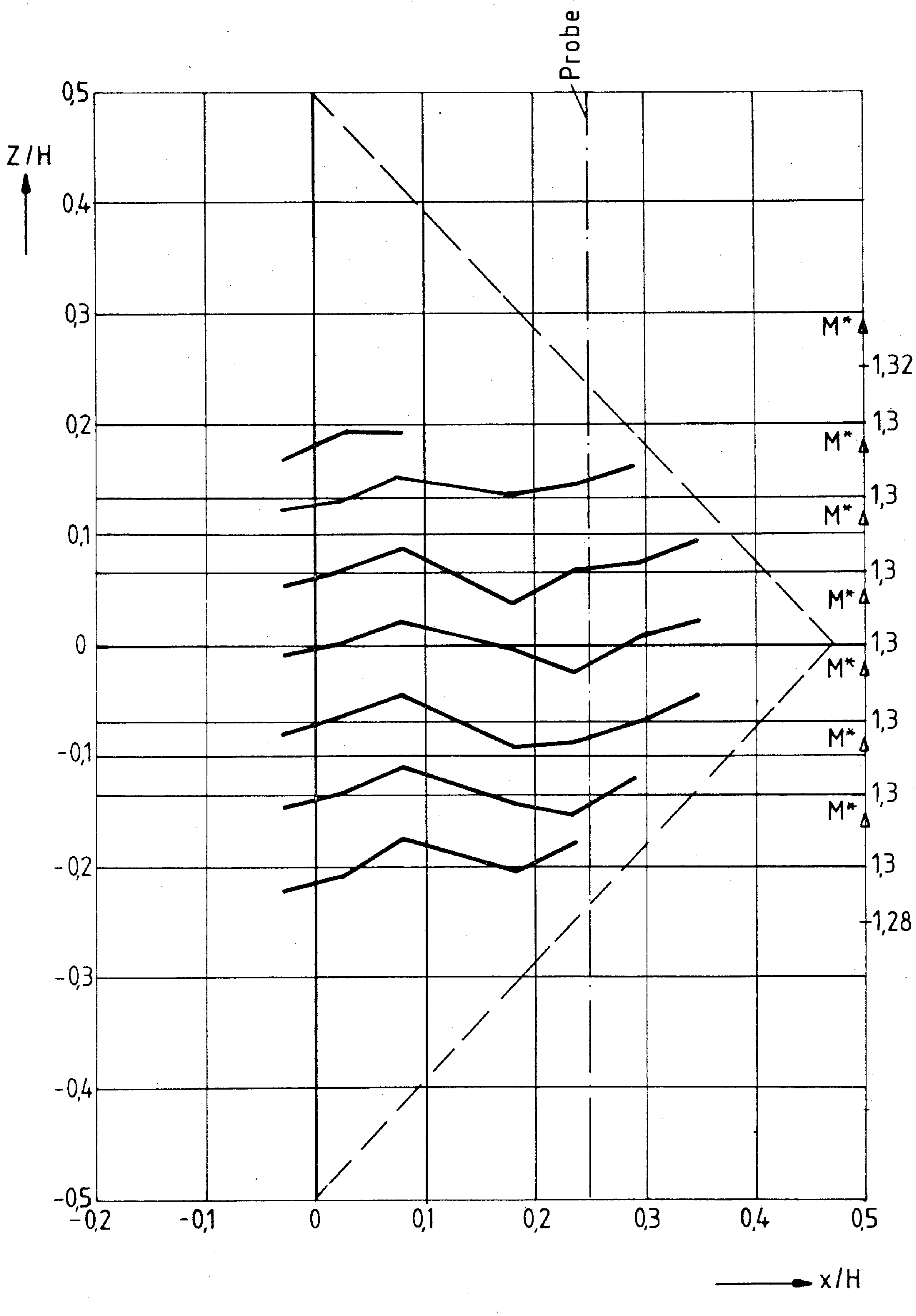

FIG. 1.3.10 M*–DISTRIBUTION NOZZLE M* = 1,3

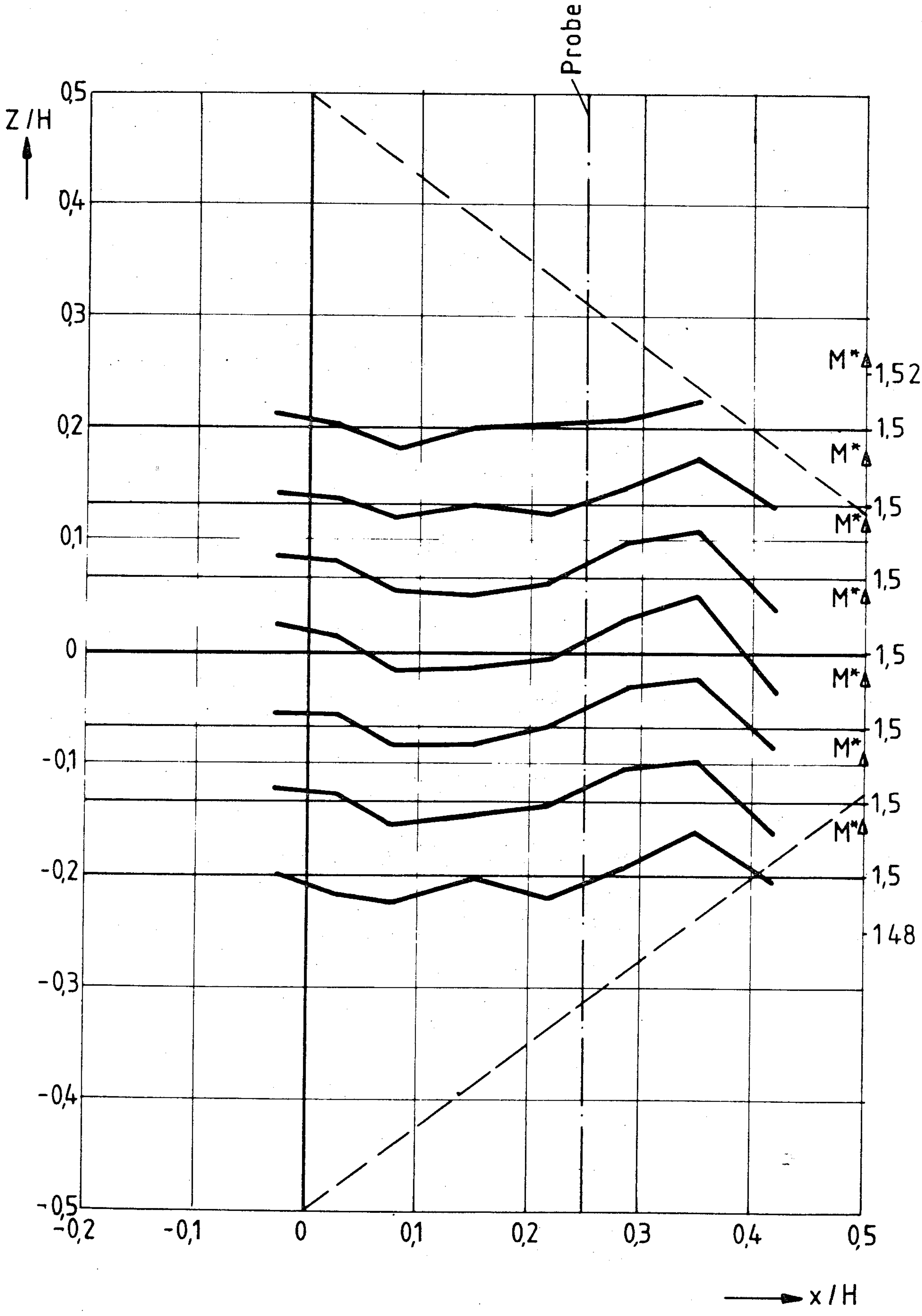

FIG. 1.3.11 M*–DISTRIBUTION NOZZLE M* = 1,5

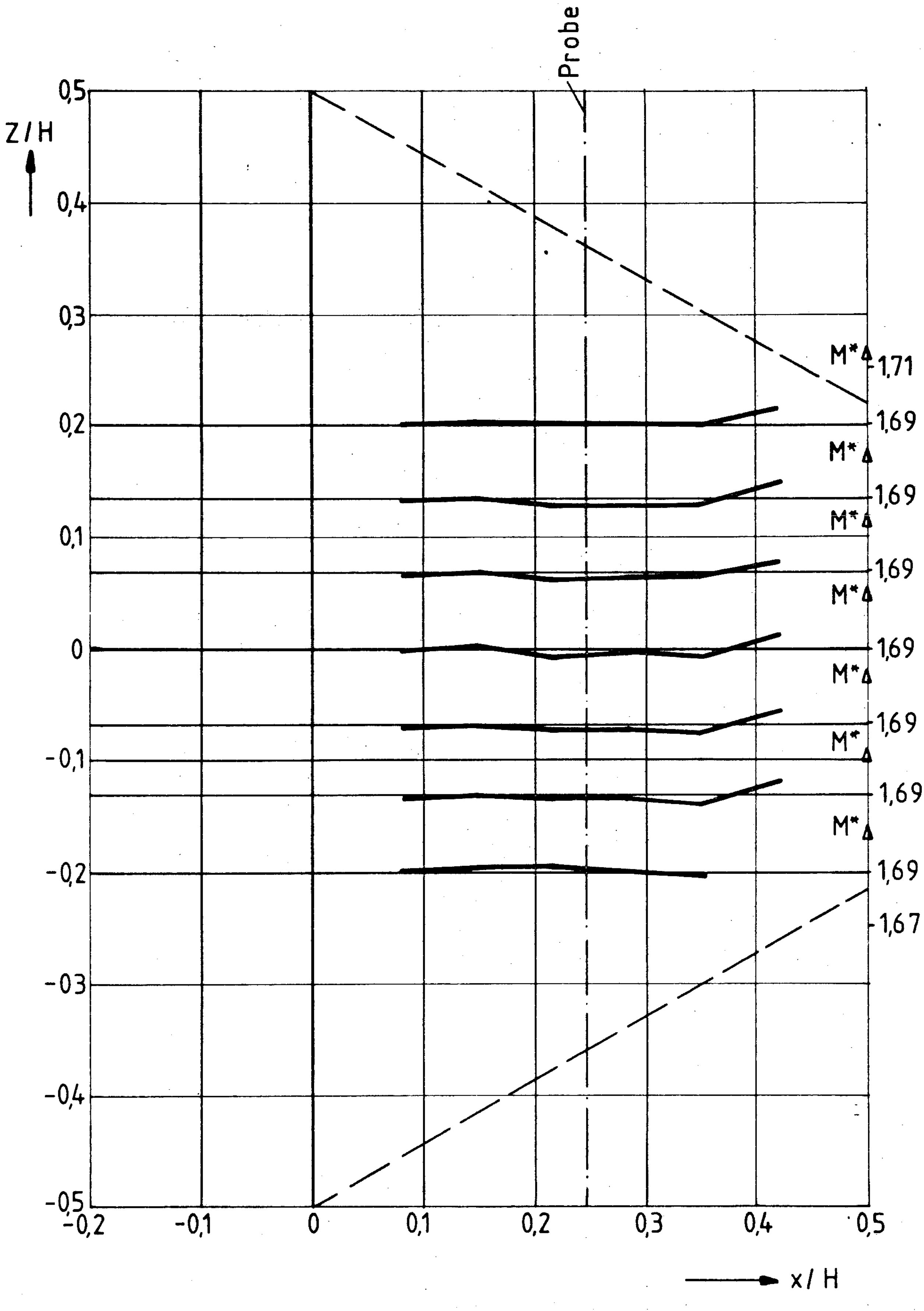

FIG. 1.3.12 M*–DISTRIBUTION NOZZLE M* = 1,7